

Axially symmetric Hartree-Fock-Bogoliubov Calculations for Nuclei Near the Drip-Lines

E. Terán,^{*} V.E. Oberacker,[†] and A.S. Umar[‡]
Department of Physics and Astronomy,
Vanderbilt University, Nashville, TN 37235, USA

(Dated: November 7, 2018)

Nuclei far from stability are studied by solving the Hartree-Fock-Bogoliubov (HFB) equations, which describe the self-consistent mean field theory with pairing interaction. Calculations for even-even nuclei are carried out on a two-dimensional axially symmetric lattice, in coordinate space. The quasiparticle continuum wavefunctions are considered for energies up to 60 MeV. Nuclei near the drip lines have a strong coupling between weakly bound states and the particle continuum. This method gives a proper description of the ground state properties of such nuclei. High accuracy is achieved by representing the operators and wavefunctions using the technique of basis-splines. The detailed representation of the HFB equations in cylindrical coordinates is discussed. Calculations of observables for nuclei near the neutron drip line are presented to demonstrate the reliability of the method.

PACS numbers: 21.60 Jz, 24.30 Cz

Keywords: Nuclear structure, HFB, Basis-splines

I. INTRODUCTION

The latest experimental developments as well as recent advances in computational physics have sparked renewed interest in nuclear structure theory. In contrast to the well-understood behavior near the valley of stability, there are many open questions as we move towards the proton and neutron driplines and towards the limits in mass number (superheavy region). The neutron dripline represents mostly “terra incognita”. In these exotic regions of the nuclear chart, one expects to see several new phenomena [1, 2]: near the neutron dripline, the neutron-matter distribution will be very diffuse and of large size giving rise to “neutron halos” and “neutrons skins”. There are also expected collective modes associated with this neutron skin, e.g. the “scissors” vibrational mode or the “pygmy” resonance. In proton-rich nuclei, we have recently seen both spherical and deformed proton emitters; this “proton radioactivity” is caused by the tunneling of weakly bound protons through the Coulomb barrier. With RIB facilities, nuclear theorists see an opportunity to study the effective N-N interaction at large isospin, as well as large pairing correlations.

It is generally acknowledged that an accurate treatment of the pairing interaction is essential for describing exotic nuclei [3, 4]. This work is specifically aimed to calculating ground state observables such as the total binding energy, charge radii, proton and neutron densities, separation energies for neutrons and protons, and pairing gaps. There are several types of approaches in nuclear structure theory [2]: for the lightest nuclei, ab-initio cal-

culations (Green’s function Monte Carlo, no-core shell model) based on the bare N-N interaction are possible [5]. Medium-mass nuclei up to $A \sim 60$ may be treated in the large-scale shell model approach [6]. For heavier nuclei one utilizes either nonrelativistic [3, 7, 8] or relativistic [9, 10, 11] mean field theories. The large pairing correlations near the driplines can no longer be described by a small residual interaction. It becomes necessary to treat the mean field and the pairing field in a single self-consistent theory. Furthermore, the outermost nucleons are weakly bound, which implies a large spatial extent, and they are strongly coupled to the particle continuum. These features represent major challenges for the mean field theories. We overcome these difficulties by solving the HFB equations for deformed, axially symmetric even-even nuclei on a two-dimensional lattice, without any further approximations. So far, most of HFB calculations are based on spherical symmetry or up to a limited energy in the quasiparticle spectrum continuum. The importance of the axially symmetry lies on the ability to emulate a big range of nuclei that are not spherical in nature, e.g. nuclei that have a non-trivial intrinsic deformation. We have developed and tested a new mean-field nuclear structure code that specifically addresses the computational challenges and opportunities presented by nuclei near the driplines.

The present work represents an introduction of the splines method to the solution of the HFB approach in axial symmetry. For now, we will focus on the methodology of our approach. We outline here briefly the theoretical and computational details. We also present results for a few nuclear systems to demonstrate the convergence of the results.

II. STANDARD HFB FORMALISM

^{*}Electronic address: edgar.teran@vanderbilt.edu

[†]Electronic address: volker.e.oberacker@vanderbilt.edu

[‡]Electronic address: umar@compsci.cas.vanderbilt.edu

The many-body Hamiltonian in occupation number representation has the form

$$\hat{H} = \sum_{i,j} \langle i|t|j\rangle \hat{c}_i^\dagger \hat{c}_j + \frac{1}{4} \sum_{i,j,m,n} \langle ij|\bar{v}^{(2)}|mn\rangle \hat{c}_i^\dagger \hat{c}_j^\dagger \hat{c}_n \hat{c}_m. \quad (2.1)$$

The general linear transformation from particle operators \hat{c}, \hat{c}^\dagger to quasiparticle operators $\hat{\beta}, \hat{\beta}^\dagger$ take the form [12]:

$$\begin{pmatrix} \hat{\beta} \\ \hat{\beta}^\dagger \end{pmatrix} = \begin{pmatrix} U^\dagger & V^\dagger \\ V^T & U^T \end{pmatrix} \begin{pmatrix} \hat{c} \\ \hat{c}^\dagger \end{pmatrix}. \quad (2.2)$$

The HFB approximate ground state of the many-body system is defined as a vacuum with respect to quasiparticles

$$\hat{\beta}_k |\Phi_0\rangle = 0.$$

The basic building blocks of the theory are the density matrix

$$\rho_{ij} = \langle \Phi_0 | \hat{c}_j^\dagger \hat{c}_i | \Phi_0 \rangle = (V^* V^T)_{ij}, \quad (2.3)$$

and the pairing tensor

$$\kappa_{ij} = \langle \Phi_0 | \hat{c}_j \hat{c}_i | \Phi_0 \rangle = (V^* U^T)_{ij}. \quad (2.4)$$

which give form to the generalized density matrix

$$\mathcal{R} = \begin{pmatrix} \rho & \kappa \\ -\kappa^* & 1 - \rho^* \end{pmatrix}.$$

The HFB ground state energy including the constraint on the particle number N is given by

$$E(\mathcal{R}) = \langle \Phi_0 | \hat{H} - \lambda \hat{N} | \Phi_0 \rangle. \quad (2.5)$$

The equations of motion are derived from the variational principle

$$\delta [E(\mathcal{R}) - \text{tr} \Lambda (\mathcal{R}^2 - \mathcal{R})] = 0, \quad (2.6)$$

which results in the standard HFB formulation

$$[\mathcal{H}, \mathcal{R}] = 0, \quad (2.7)$$

with the generalized single-particle Hamiltonian

$$\mathcal{H} = \begin{pmatrix} (h - \lambda) & \Delta \\ -\Delta^* & -(h - \lambda)^* \end{pmatrix}, \quad (2.8)$$

where h and Δ denote the mean field Hamiltonian and pairing potential, respectively, and the Lagrange multiplier λ is the Fermi energy of the system.

A. Quasiparticle wavefunctions in coordinate space

In practice, it is convenient to transform the standard HFB equations into a coordinate space representation and solve the resulting differential equations on a lattice. For this purpose, we define two types of quasiparticle wavefunctions ϕ_1 and ϕ_2 , corresponding to each quasiparticle energy state E_α :

$$\phi_1^*(E_\alpha, \mathbf{r}\sigma q) = \sum_i U_{i\alpha} (2\sigma) \phi_i(\mathbf{r} - \sigma q), \quad (2.9a)$$

$$\phi_2(E_\alpha, \mathbf{r}\sigma q) = \sum_i V_{i\alpha}^* \phi_i(\mathbf{r}\sigma q). \quad (2.9b)$$

The basis wavefunctions ϕ_i depend on the coordinate vector \mathbf{r} , the spin projection $\sigma = \pm \frac{1}{2}$, and the isospin projection q ($q = +\frac{1}{2}$ corresponds to protons and $q = -\frac{1}{2}$ to neutrons).

The particle density matrix for the HFB ground state assumes a very simple mathematical structure in terms of ϕ_1 and ϕ_2 [4]:

$$\begin{aligned} \rho(\mathbf{r}\sigma q, \mathbf{r}'\sigma'q') &= \langle \Phi_0 | \hat{\psi}^\dagger(\mathbf{r}'\sigma'q') \hat{\psi}(\mathbf{r}\sigma q) | \Phi_0 \rangle \\ &= \sum_{i,j} \rho_{ij} \phi_i(\mathbf{r}\sigma q) \phi_j^*(\mathbf{r}'\sigma'q') \\ &= \sum_{E_\alpha > 0}^{\infty} \phi_2(E_\alpha, \mathbf{r}\sigma q) \phi_2^*(E_\alpha, \mathbf{r}'\sigma'q'). \end{aligned} \quad (2.10)$$

The sum over the states E_α has replaced the integral form of the equations, since the HFB continuous spectrum has been discretized for practical calculations. Instead of the standard antisymmetric pairing tensor κ defined as

$$\kappa(\mathbf{r}\sigma q, \mathbf{r}'\sigma'q') = \langle \Phi_0 | \hat{\psi}(\mathbf{r}'\sigma'q') \hat{\psi}(\mathbf{r}\sigma q) | \Phi_0 \rangle \quad (2.11)$$

we introduce the pairing density matrix $\tilde{\rho}$ which is Hermitian for a time-reversal invariant ground state and hence more convenient to use [4]:

$$\begin{aligned} \tilde{\rho}(\mathbf{r}\sigma q, \mathbf{r}'\sigma'q') &= (-2\sigma') \kappa(\mathbf{r}\sigma q, \mathbf{r}' - \sigma'q') \\ &= (-2\sigma') \sum_{i,j} \kappa_{ij} \phi_i(\mathbf{r}\sigma q) \phi_j(\mathbf{r}' - \sigma'q') \\ &= - \sum_{E_\alpha > 0}^{\infty} \phi_2(E_\alpha, \mathbf{r}\sigma q) \phi_1^*(E_\alpha, \mathbf{r}'\sigma'q'). \end{aligned} \quad (2.12)$$

In principle, the sums go over all the energy states, but in practice a cutoff in the number of states is done up to a reasonable number (~ 60 MeV).

Proceeding in analogy to the pairing density matrix, we replace the antisymmetric pairing potential Δ in Eq. (2.8) with the Hermitian pairing field \tilde{h}

$$\tilde{h}(\mathbf{r}\sigma q, \mathbf{r}'\sigma'q') = (-2\sigma') \Delta(\mathbf{r}\sigma q, \mathbf{r}' - \sigma'q'). \quad (2.13)$$

B. Normal density and pairing density

From expressions (2.10) and (2.12) for the density matrices we obtain the following expressions for the normal density $\rho_q(\mathbf{r})$ and pairing density $\tilde{\rho}_q(\mathbf{r})$, which are defined as the spin-averaged diagonal elements of their correspondent matrices

$$\begin{aligned}\rho_q(\mathbf{r}) &= \sum_{\sigma} \rho(\mathbf{r}\sigma q, \mathbf{r}\sigma q) \\ &= \sum_{\sigma} \sum_{\alpha} \phi_{2,\alpha}(\mathbf{r}\sigma q) \phi_{2,\alpha}^*(\mathbf{r}\sigma q),\end{aligned}\quad (2.14)$$

$$\begin{aligned}\tilde{\rho}_q(\mathbf{r}) &= \sum_{\sigma} \tilde{\rho}(\mathbf{r}\sigma q, \mathbf{r}\sigma q) \\ &= -\sum_{\sigma} \sum_{\alpha} \phi_{2,\alpha}(\mathbf{r}\sigma q) \phi_{1,\alpha}^*(\mathbf{r}\sigma q).\end{aligned}\quad (2.15)$$

The quasiparticle energy E_{α} is denoted by index α for simplicity. The physical interpretation of $\tilde{\rho}_q$ has been discussed in [4]: the quantity $[\tilde{\rho}_q(\mathbf{r}) \Delta V/2]^2$ gives the probability to find a *correlated* pair of nucleons with opposite spin projection in the volume element ΔV .

C. Kinetic and spin-orbit densities

The kinetic energy density $\tau_q(\mathbf{r})$ is defined as a functional of wavefunctions ϕ_2

$$\begin{aligned}\tau_q(\mathbf{r}) &= \nabla \cdot \nabla' \rho_q(\mathbf{r}, \mathbf{r}')|_{\mathbf{r}=\mathbf{r}'} \\ &= \nabla \cdot \nabla' \left(\sum_{\sigma} \rho(\mathbf{r}\sigma q, \mathbf{r}'\sigma q) \right) |_{\mathbf{r}=\mathbf{r}'} \\ &= \sum_{\sigma} \sum_{\alpha} |\nabla \phi_{2,\alpha}(\mathbf{r}\sigma q)|^2.\end{aligned}\quad (2.16)$$

$$h(\mathbf{r}\sigma, \mathbf{r}'\sigma') = t(\mathbf{r}\sigma, \mathbf{r}'\sigma') + \int d^3 r_2 \int d^3 r_2' \sum_{\sigma_2, \sigma_2'} \bar{v}^{(2)}(\mathbf{r}\sigma, \mathbf{r}_2\sigma_2; \mathbf{r}'\sigma', \mathbf{r}_2'\sigma_2') \rho(\mathbf{r}_2'\sigma_2', \mathbf{r}_2\sigma_2). \quad (2.20)$$

where $\bar{v}_{12}^{(2)}$ is the antisymmetrized two-body effective N-N interaction (see Appendix). The kinetic energy matrix elements are given by

$$t(\mathbf{r}\sigma, \mathbf{r}'\sigma') = \delta(\mathbf{r} - \mathbf{r}') \delta_{\sigma, \sigma'} \left(-\frac{\hbar^2}{2m} \nabla^2 \right). \quad (2.21)$$

E. Pairing interaction

In practice, one tends to use *different* effective N-N interactions for the p-h and for the p-p channel. If one

The spin-orbit density does not appear directly in the nuclear potential, but rather its divergence

$$\nabla \cdot \mathbf{J}_q(\mathbf{r}) = -i \sum_{\alpha} (\nabla \phi_{2,\alpha}^{\dagger}(\mathbf{r}, q)) \cdot (\nabla \times \sigma) \phi_{2,\alpha}(\mathbf{r}, q). \quad (2.17)$$

D. Energy functional and mean fields

Standard HFB theory yields the following expression for the total binding energy of the nucleus in its ground state, with contributions from the mean field and the pairing field

$$E_{HFB} = \langle \Phi_{HFB} | \hat{H} | \Phi_{HFB} \rangle = E_{mf} + E_{pair}.$$

To simplify the notation, we drop the isospin indices q, q' in this section and in the following section. In coordinate space, the mean field contribution is given by [4]

$$\begin{aligned}E_{mf} &= \frac{1}{2} \int d^3 r \int d^3 r' \sum_{\sigma, \sigma'} [t(\mathbf{r}\sigma, \mathbf{r}'\sigma') + h(\mathbf{r}\sigma, \mathbf{r}'\sigma')] \\ &\quad \times \rho(\mathbf{r}'\sigma', \mathbf{r}\sigma),\end{aligned}\quad (2.18)$$

and pairing energy contribution has the form

$$E_{pair} = \frac{1}{2} \int d^3 r \int d^3 r' \sum_{\sigma, \sigma'} \tilde{h}(\mathbf{r}\sigma, \mathbf{r}'\sigma') \tilde{\rho}(\mathbf{r}'\sigma', \mathbf{r}\sigma). \quad (2.19)$$

The quantity h denotes the mean field, i.e. the particle-hole (p-h) channel of the interaction

In a similar way, we find for the pairing mean field \tilde{h} , i.e. for the p-p and h-h channels of the interaction

$$\tilde{h}(\mathbf{r}\sigma, \mathbf{r}'\sigma') = \int d^3 r_1' \int d^3 r_2' \sum_{\sigma_1', \sigma_2'} 2\sigma_1' \sigma_2' \bar{v}_{pair}^{(2)}(\mathbf{r}\sigma, \mathbf{r}' - \sigma'; \mathbf{r}_1' \sigma_1', \mathbf{r}_2' - \sigma_2') \tilde{\rho}(\mathbf{r}_1' \sigma_1', \mathbf{r}_2' \sigma_2'). \quad (2.22)$$

assumes that the effective interaction $\bar{v}_{pair}^{(2)}$ is local

$$\begin{aligned}\bar{v}_{pair}^{(2)}(\mathbf{r}\sigma, \mathbf{r}' - \sigma'; \mathbf{r}_1' \sigma_1', \mathbf{r}_2' - \sigma_2') &= \delta(\mathbf{r}_1' - \mathbf{r}) \delta_{\sigma_1', \sigma} \\ &\quad \times \delta(\mathbf{r}_2' - \mathbf{r}') \delta_{\sigma_2', \sigma'} V_p(\mathbf{r}\sigma, \mathbf{r}' - \sigma'),\end{aligned}$$

the pairing mean field Hamiltonian becomes

$$\tilde{h}(\mathbf{r}\sigma, \mathbf{r}'\sigma') = V_p(\mathbf{r}\sigma, \mathbf{r}' - \sigma') \tilde{\rho}(\mathbf{r}\sigma, \mathbf{r}'\sigma') .$$

For the pairing interaction V_p we utilize the form

$$V_p(\mathbf{r}\sigma, \mathbf{r}' - \sigma') = V_0 \delta(\mathbf{r} - \mathbf{r}') \delta_{\sigma, \sigma'} F(\mathbf{r}) .$$

This parameterization describes two primary pairing forces: a pure delta interaction ($F = 1$) that gives rise to *volume pairing*, and a density dependent delta interaction (DDDI) that gives rise to *surface pairing*. In the latter case, one uses the following phenomenological ansatz [20] for the factor F

$$F(\mathbf{r}) = 1 - \left(\frac{\rho(\mathbf{r})}{\rho_0} \right)^\gamma \quad (2.23)$$

where $\rho(\mathbf{r})$ is the mass density.

The DDDI interaction generates the following pairing mean field for the two isospin orientations $q = \pm \frac{1}{2}$

$$\tilde{h}_q(\mathbf{r}\sigma, \mathbf{r}'\sigma') = \frac{1}{2} V_0^{(q)} \tilde{\rho}_q(\mathbf{r}) F(\mathbf{r}) \delta(\mathbf{r} - \mathbf{r}') \delta_{\sigma, \sigma'} . \quad (2.24)$$

The pairing contribution to the nuclear binding energy is then

$$\begin{aligned} E_{pair} &= E_{pair}^{(p)} + E_{pair}^{(n)} \\ &= \int d^3r \left[\frac{V_0^{(p)}}{4} \tilde{\rho}_p^2(\mathbf{r}) + \frac{V_0^{(n)}}{4} \tilde{\rho}_n^2(\mathbf{r}) \right] F(\mathbf{r}) . \end{aligned}$$

An important related quantity is the average pairing gap for protons and neutrons which is defined as [3, 4]

$$\begin{aligned} \langle \Delta_q \rangle &= -\frac{1}{N_q} \text{trace} \left(\tilde{h}_q \rho_q \right) \\ &= -\frac{1}{N_q} \int d^3r \int d^3r' \sum_{\sigma, \sigma'} \tilde{h}_q(\mathbf{r}\sigma, \mathbf{r}'\sigma') \rho_q(\mathbf{r}'\sigma', \mathbf{r}\sigma) \end{aligned}$$

where N_q denotes the number of protons or neutrons. Inserting the expression derived earlier for the mean pairing field we arrive at

$$\langle \Delta_q \rangle = -\frac{1}{2} \frac{V_0^{(q)}}{N_q} \int d^3r \tilde{\rho}_q(\mathbf{r}) \rho_q(\mathbf{r}) F(\mathbf{r}) . \quad (2.25)$$

Note that the pairing gap is a positive quantity because $V_0^{(q)} < 0$.

F. HFB equations in coordinate space

For certain types of effective interactions (e.g. Skyrme mean field and pairing delta-interactions) the particle Hamiltonian h and the pairing Hamiltonian \tilde{h} are diagonal in isospin space and local in position space,

$$h(\mathbf{r}\sigma q, \mathbf{r}'\sigma' q') = \delta_{q, q'} \delta(\mathbf{r} - \mathbf{r}') h_{\sigma, \sigma'}^q(\mathbf{r}) \quad (2.26a)$$

and

$$\tilde{h}(\mathbf{r}\sigma q, \mathbf{r}'\sigma' q') = \delta_{q, q'} \delta(\mathbf{r} - \mathbf{r}') \tilde{h}_{\sigma, \sigma'}^q(\mathbf{r}) . \quad (2.26b)$$

Inserting these into the above HFB equations results in a 4x4 structure in spin space:

$$\begin{pmatrix} (h^q - \lambda) & \tilde{h}^q \\ \tilde{h}^q & -(h^q - \lambda) \end{pmatrix} \begin{pmatrix} \phi_{1, \alpha}^q \\ \phi_{2, \alpha}^q \end{pmatrix} = E_\alpha \begin{pmatrix} \phi_{1, \alpha}^q \\ \phi_{2, \alpha}^q \end{pmatrix} \quad (2.27)$$

with

$$h^q = \begin{pmatrix} h_{\uparrow\uparrow}^q(\mathbf{r}) & h_{\uparrow\downarrow}^q(\mathbf{r}) \\ h_{\downarrow\uparrow}^q(\mathbf{r}) & h_{\downarrow\downarrow}^q(\mathbf{r}) \end{pmatrix}, \quad \tilde{h}^q = \begin{pmatrix} \tilde{h}_{\uparrow\uparrow}^q(\mathbf{r}) & \tilde{h}_{\uparrow\downarrow}^q(\mathbf{r}) \\ \tilde{h}_{\downarrow\uparrow}^q(\mathbf{r}) & \tilde{h}_{\downarrow\downarrow}^q(\mathbf{r}) \end{pmatrix} .$$

Because of the structural similarity between the Dirac equation and the HFB equation in coordinate space, we encounter here similar computational challenges: for example, the spectrum of quasiparticle energies E is unbounded from above *and* below. The spectrum is discrete for $|E| < -\lambda$ and continuous for $|E| > -\lambda$. For even-even nuclei it is customary to solve the HFB equations with a positive quasiparticle energy spectrum $+E_\alpha$ and consider all negative energy states as occupied in the HFB ground state.

III. 2-D REDUCTION FOR AXIALLY SYMMETRIC SYSTEMS

For simplicity, we assume that the HFB quasiparticle Hamiltonian is invariant under rotations \hat{R}_z around the z-axis, i.e. $[\mathcal{H}, \hat{R}_z] = 0$. Due to the axial symmetry of the problem, it is advantageous to introduce cylindrical coordinates (ϕ, r, z) . It is possible to construct simultaneous eigenfunctions of the generalized Hamiltonian \mathcal{H} and the z-component of the angular momentum, \hat{j}_z

$$\mathcal{H} \psi_{n, \Omega, q}(\phi, r, z) = E_{n, \Omega, q} \psi_{n, \Omega, q}(\phi, r, z) \quad (3.1a)$$

$$\hat{j}_z \psi_{n, \Omega, q}(\phi, r, z) = \hbar \Omega \psi_{n, \Omega, q}(\phi, r, z) , \quad (3.1b)$$

with quantum numbers $\Omega = \pm \frac{1}{2}, \pm \frac{3}{2}, \pm \frac{5}{2}, \dots$ corresponding to each n th energy state. The simultaneous quasiparticle eigenfunctions take the form

$$\begin{aligned} \psi_{n, \Omega, q}(\phi, r, z) &= \begin{pmatrix} \phi_{n, \Omega, q}^{(1)}(\phi, r, z) \\ \phi_{n, \Omega, q}^{(2)}(\phi, r, z) \end{pmatrix} \\ &= \frac{1}{\sqrt{2\pi}} \begin{pmatrix} e^{i(\Omega - \frac{1}{2})\phi} \phi_{n, \Omega, q}^{(1)}(r, z, \uparrow) \\ e^{i(\Omega + \frac{1}{2})\phi} \phi_{n, \Omega, q}^{(1)}(r, z, \downarrow) \\ e^{i(\Omega - \frac{1}{2})\phi} \phi_{n, \Omega, q}^{(2)}(r, z, \uparrow) \\ e^{i(\Omega + \frac{1}{2})\phi} \phi_{n, \Omega, q}^{(2)}(r, z, \downarrow) \end{pmatrix} \quad (3.2) \end{aligned}$$

We introduce the following useful notation

$$U_{n\Omega q}^{(1,2)}(r, z) = \phi_{n, \Omega, q}^{(1,2)}(r, z, \uparrow) , \quad (3.3a)$$

$$L_{n\Omega q}^{(1,2)}(r, z) = \phi_{n, \Omega, q}^{(1,2)}(r, z, \downarrow) . \quad (3.3b)$$

From the vanishing commutator, $[\mathcal{H}, j_z]$, we can determine the ϕ -dependence of the HFB quasiparticle Hamiltonian and arrive at the following structure for the Hamiltonian

$$h(\phi, r, z) = \begin{pmatrix} h'_{\uparrow\uparrow}(r, z) & e^{-i\phi} h'_{\uparrow\downarrow}(r, z) \\ e^{+i\phi} h'_{\downarrow\uparrow}(r, z) & h'_{\downarrow\downarrow}(r, z) \end{pmatrix}. \quad (3.4)$$

and the pairing Hamiltonian

$$\tilde{h}(\phi, r, z) = \begin{pmatrix} \tilde{h}'_{\uparrow\uparrow}(r, z) & e^{-i\phi} \tilde{h}'_{\uparrow\downarrow}(r, z) \\ e^{+i\phi} \tilde{h}'_{\downarrow\uparrow}(r, z) & \tilde{h}'_{\downarrow\downarrow}(r, z) \end{pmatrix}, \quad (3.5)$$

Inserting equations (3.4) and (3.5) into the eigenvalue Eq. (2.27), we arrive at the *reduced 2-D problem* in cylindrical coordinates:

$$\begin{pmatrix} (h'_{\uparrow\uparrow} - \lambda) & h'_{\uparrow\downarrow} & \tilde{h}'_{\uparrow\uparrow} & \tilde{h}'_{\uparrow\downarrow} \\ h'_{\downarrow\uparrow} & (h'_{\downarrow\downarrow} - \lambda) & \tilde{h}'_{\downarrow\uparrow} & \tilde{h}'_{\downarrow\downarrow} \\ \tilde{h}'_{\uparrow\uparrow} & \tilde{h}'_{\uparrow\downarrow} & -(h'_{\uparrow\uparrow} - \lambda) & -h'_{\uparrow\downarrow} \\ \tilde{h}'_{\downarrow\uparrow} & \tilde{h}'_{\downarrow\downarrow} & -h'_{\downarrow\uparrow} & -(h'_{\downarrow\downarrow} - \lambda) \end{pmatrix} \times \begin{pmatrix} U_{n,\Omega,q}^{(1)} \\ L_{n,\Omega,q}^{(1)} \\ U_{n,\Omega,q}^{(2)} \\ L_{n,\Omega,q}^{(2)} \end{pmatrix} = E_{n,\Omega,q} \begin{pmatrix} U_{n,\Omega,q}^{(1)} \\ L_{n,\Omega,q}^{(1)} \\ U_{n,\Omega,q}^{(2)} \\ L_{n,\Omega,q}^{(2)} \end{pmatrix} \quad (3.6)$$

Here, quantities \tilde{h}' , h' , U and L are all functions of (r, z) only. Also, \tilde{h}' and h' contain the implicit isospin dependence q . This is the main mathematical structure that we implement in computational calculations. For a given angular momentum projection quantum number Ω , we solve the eigenvalue problem to obtain energy eigenvalues $E_{n,\Omega,q}$ and eigenvectors $\psi_{n,\Omega,q}$ for the corresponding HFB quasiparticle states.

A. Representation of operators

The Hartree-Fock Hamiltonian using the Skyrme effective interaction can be written

$$h_q = -\nabla \cdot \frac{\hbar^2}{2m_q^*} \nabla + U_q + U_C \delta_{q\frac{1}{2}} + \frac{1}{2i} (\nabla \cdot \mathbf{I}_q + \mathbf{I}_q \cdot \nabla) - i\mathbf{B}_q \cdot (\nabla \times \sigma) \quad (3.7)$$

where U_q is the nuclear central field, U_C the Coulomb interaction, and the spin-orbit field part is given by $\mathbf{B}_q \cdot (\nabla \times \sigma)$. The explicit form of these expressions for the case of the Skyrme interaction are included in the Appendix. Starting from the kinetic energy we apply the cylindrical form of the Laplacian operator to the standard form of the wavefunction in Eq.(3.2), to find

$$\hat{t}_q = \begin{pmatrix} t_{11} & 0 \\ 0 & t_{22} \end{pmatrix}, \quad (3.8)$$

whose elements are given by

$$t_{11} = f \left(\frac{\partial^2}{\partial r^2} + \frac{1}{r} \frac{\partial}{\partial r} - \left(\frac{(\Omega - 1/2)}{r} \right)^2 + \frac{\partial^2}{\partial z^2} \right) + \frac{\partial f}{\partial r} \frac{\partial}{\partial r} + \frac{\partial f}{\partial z} \frac{\partial}{\partial z} \quad (3.9a)$$

$$t_{22} = f \left(\frac{\partial^2}{\partial r^2} + \frac{1}{r} \frac{\partial}{\partial r} - \left(\frac{(\Omega + 1/2)}{r} \right)^2 + \frac{\partial^2}{\partial z^2} \right) + \frac{\partial f}{\partial r} \frac{\partial}{\partial r} + \frac{\partial f}{\partial z} \frac{\partial}{\partial z}, \quad (3.9b)$$

f being the effective mass given in (A.9). The local potential terms could also be cast into a matrix form

$$\hat{v}_q = \begin{pmatrix} v_{11} & 0 \\ 0 & v_{22} \end{pmatrix}, \quad (3.10)$$

where

$$v_{11} = v_{22} = U_q + U_C \delta_{q\frac{1}{2}}. \quad (3.11)$$

Expressions for U_q and U_C are given in the Appendix. The Hartree-Fock spin-orbit operator

$$-i\mathbf{B}_q \cdot (\nabla \times \sigma) \longrightarrow \hat{w}_q, \quad (3.12)$$

can similarly be written into the form

$$\hat{w}_q = \begin{pmatrix} w_{11} & w_{12} \\ w_{21} & w_{22} \end{pmatrix}, \quad (3.13)$$

with [15]

$$w_{11} = \mathcal{B}_r \frac{\Omega - 1/2}{r} \quad (3.14a)$$

$$w_{12} = \left[-\mathcal{B}_z \frac{\Omega + 1/2}{r} - \mathcal{B}_z \frac{\partial}{\partial r} + \mathcal{B}_r \frac{\partial}{\partial z} \right] \quad (3.14b)$$

$$w_{21} = \left[-\mathcal{B}_z \frac{\Omega - 1/2}{r} + \mathcal{B}_z \frac{\partial}{\partial r} - \mathcal{B}_r \frac{\partial}{\partial z} \right] \quad (3.14c)$$

$$w_{22} = -\mathcal{B}_r \frac{\Omega + 1/2}{r}, \quad (3.14d)$$

where $\mathcal{B}_r, \mathcal{B}_z$ are defined in the Appendix for the Skyrme force.

B. Densities and currents

Making use of the definitions for the normal density and pairing density, Eqs. (2.14) and (2.15), we apply the bi-spinor structure of the quasiparticle wavefunctions to find the corresponding expressions in axial symmetry:

$$\rho_q(r, z) = \frac{1}{2\pi} \left(2 \sum_{\Omega>0}^{\Omega_{max}} \right) \times \sum_{E_n>0}^{E_{max}} \left[|U_{n\Omega q}^{(2)}(r, z)|^2 + |L_{n\Omega q}^{(2)}(r, z)|^2 \right] \quad (3.15)$$

$$\tilde{\rho}_q(r, z) = -\frac{1}{2\pi} \left(2 \sum_{\Omega>0}^{\Omega_{max}} \right) \times \sum_{E_n>0}^{E_{max}} \left[U_{n\Omega q}^{(2)}(r, z) U_{n\Omega q}^{(1)*}(r, z) + L_{n\Omega q}^{(2)}(r, z) L_{n\Omega q}^{(1)*}(r, z) \right]. \quad (3.16)$$

Similarly, starting from definitions (2.16) and (2.17), we obtain expressions for the kinetic energy density and the divergence of the current

$$\begin{aligned} \tau_q(r, z) = \frac{1}{2\pi} \left(2 \sum_{\Omega>0}^{\Omega_{max}} \right) \sum_{E_n>0}^{E_{max}} \left[\frac{(\Omega - 1/2)^2}{r^2} |U_{n\Omega q}^{(2)}|^2 + \frac{(\Omega + 1/2)^2}{r^2} |L_{n\Omega q}^{(2)}|^2 \right. \\ \left. + \left| \frac{\partial U_{n\Omega q}^{(2)}}{\partial r} \right|^2 + \left| \frac{\partial L_{n\Omega q}^{(2)}}{\partial r} \right|^2 + \left| \frac{\partial U_{n\Omega q}^{(2)}}{\partial z} \right|^2 + \left| \frac{\partial L_{n\Omega q}^{(2)}}{\partial z} \right|^2 \right], \end{aligned} \quad (3.17)$$

$$\begin{aligned} \nabla \cdot \mathbf{J}_q(\mathbf{r}) = \frac{1}{2\pi} \left(2 \sum_{\Omega>0}^{\Omega_{max}} \right) \sum_{E_n>0}^{E_{max}} 2 \left[\frac{\partial U_{n\Omega q}^{(2)}}{\partial r} \frac{\partial L_{n\Omega q}^{(2)}}{\partial z} - \frac{\partial L_{n\Omega q}^{(2)}}{\partial r} \frac{\partial U_{n\Omega q}^{(2)}}{\partial z} + \frac{\Omega - 1/2}{r} U_{n\Omega q}^{(2)} \left(\frac{\partial U_{n\Omega q}^{(2)}}{\partial r} - \frac{\partial L_{n\Omega q}^{(2)}}{\partial z} \right) \right. \\ \left. - \frac{\Omega + 1/2}{r} L_{n\Omega q}^{(2)} \left(\frac{\partial U_{n\Omega q}^{(2)}}{\partial z} + \frac{\partial L_{n\Omega q}^{(2)}}{\partial r} \right) \right]. \end{aligned} \quad (3.18)$$

The total number of protons or neutrons is obtained by integrating their densities

$$N_q = \int d^3r \rho_q(\mathbf{r}) = \left(2 \sum_{\Omega>0}^{\Omega_{max}} \right) \sum_{E_n>0}^{E_{max}} N_{n\Omega q} \quad (3.19)$$

with

$$N_{n\Omega q} = \int_0^\infty r dr \int_{-\infty}^\infty dz \left[|U_{n\Omega q}^{(2)}(r, z)|^2 + |L_{n\Omega q}^{(2)}(r, z)|^2 \right] \quad (3.20)$$

which gives the contribution of the quasiparticle state $|n\Omega q \rangle$ to the proton or neutron density. In the HF+BCS limit, $N_{n\Omega q} \rightarrow v_{n\Omega q}^2$. An analogous treatment of the pairing density yields

$$P_q = \int d^3r \tilde{\rho}_q(\mathbf{r}) = \left(2 \sum_{\Omega>0}^{\Omega_{max}} \right) \sum_{E_n>0}^{E_{max}} P_{n\Omega q} \quad (3.21)$$

with the ‘‘pairing density spectral distribution’’ (with respect to energy and angular momentum)

$$\begin{aligned} P_{n\Omega q} = - \int_0^\infty r dr \int_{-\infty}^\infty dz \left[U_{n\Omega q}^{(2)}(r, z) U_{n\Omega q}^{(1)*}(r, z) \right. \\ \left. + L_{n\Omega q}^{(2)}(r, z) L_{n\Omega q}^{(1)*}(r, z) \right] \end{aligned} \quad (3.22)$$

In the HF+BCS limit, $P_{n\Omega q} \rightarrow (u \cdot v)_{n\Omega q}$. Finally, we state the normalization condition for the four-spinor quasiparticle wavefunctions as

$$\int d^3r \psi_{n\Omega q}^\dagger(\mathbf{r}) \psi_{n\Omega q}(\mathbf{r}) = 1, \quad (3.23)$$

which leads to

$$\int_0^\infty r dr \int_{-\infty}^\infty dz \left[|U_{n\Omega q}^{(1)}(r, z)|^2 + |L_{n\Omega q}^{(1)}(r, z)|^2 + |U_{n\Omega q}^{(2)}(r, z)|^2 + |L_{n\Omega q}^{(2)}(r, z)|^2 \right] = 1. \quad (3.24)$$

IV. LATTICE REPRESENTATION OF SPINOR WAVEFUNCTIONS AND HAMILTONIAN

For axially symmetric nuclei, we diagonalize the HFB Hamiltonian (3.6) separately for fixed isospin projection q and angular momentum quantum number Ω . We solve the eigenvalue problem by direct diagonalization on a two-dimensional grid (r_α, z_β) , where $\alpha = 1, \dots, N_r$ and $\beta = 1, \dots, N_z$. (Because the grid usually extends from $-z$ to $+z$, we have $N_r \approx N_z$, so when referring to the number of points in the mesh we only mention the values of N_r). The four components of the spinor wavefunction $\psi(r, z)$ are represented on the two-dimensional lattice by an expansion in Basis-Spline functions $B_i(x)$ evaluated at the lattice support points. Further details about the Basis-Spline technique are given in Refs. [13, 14]. For the lattice representation of the Hamiltonian, we use a hybrid method [15, 16, 17] in which derivative operators are constructed using the Galerkin method; this amounts to a global error reduction. Local potentials are represented by the Basis-Spline collocation method (local error reduction). The lattice representation transforms the

differential operator equation into a matrix form

$$\sum_{\nu=1}^N \mathcal{H}_n^\nu \psi_\nu^\Omega = E_n^\Omega \psi_n^\Omega \quad (n = 1, \dots, N), \quad (4.1)$$

The HFB calculations are initialized using the density output from a prior *HF+BCS* run which results in fast convergence of the HFB code. Because the HFB problem is self-consistent we use an iterative method for the solution, and at every iteration the full HFB Hamiltonian is diagonalized. Typically 15-20 iterations are sufficient for convergence at the level of one part in 10^5 for the total binding energy. The Fermi levels λ_q for protons and neutrons are calculated in every iteration by means of a simple root search using the equations [3]

$$\begin{aligned} f(\lambda_q) &= \bar{N}_q(\lambda_q) - N_q = 0 \\ \bar{N}_q(\lambda_q) &= \left(2 \sum_{\Omega>0}^{\Omega_{max}} \right) \sum_{E_n>0}^{E_{max}} \bar{N}_{n\Omega q}(\lambda_q) \\ \bar{N}_{n\Omega q}(\lambda_q) &= \frac{1}{2} \left[1 - \frac{(\mathcal{E}_{n\Omega q} - \lambda_q)}{((\mathcal{E}_{n\Omega q} - \lambda_q)^2 + \Delta_{n\Omega q}^2)^{\frac{1}{2}}} \right] \\ \Delta_{n\Omega q} &= 2 E_{n\Omega q} \sqrt{N_{n\Omega q}(1 - N_{n\Omega q})}, \quad (4.2) \end{aligned}$$

where E denotes the quasiparticle energy, and \mathcal{E} is the equivalent single-particle energy (as defined by the BCS formalism). The quantity N in the last line of the equation denotes the spectral norm of the density as defined in Eq. 3.20. The calculated value for λ_q is used in the next iteration. This process is repeated until convergence is achieved.

V. NUMERICAL PARAMETERS: ^{22}O CALCULATIONS

In this section, we present a series of studies of the numerical parameters in axially symmetric HFB calculations. In particular, we study the dependence of observables on the equivalent single particle energy cut-off, the lattice box size, the number of mesh points, and the maximum angular momentum quantum number Ω_{max} . The numerical tests are carried out for ^{22}O . This neutron-rich isotope has an N/Z ratio of 1.75 and is close to the experimentally confirmed dripline nucleus ^{24}O .

A. Energy cutoff

The numerical solution of the HFB equations on a 2-D lattice results in a set of quasiparticle wavefunctions and energies. The quasiparticle energy spectrum contains both bound and (discretized) continuum states. The number of eigenstates is determined by the dimensionality of the discrete HFB Hamiltonian, which is $N = (4 \cdot N_r \cdot N_z)^2$, for fixed isospin projection q and angular momentum projection Ω . In our calculations, we

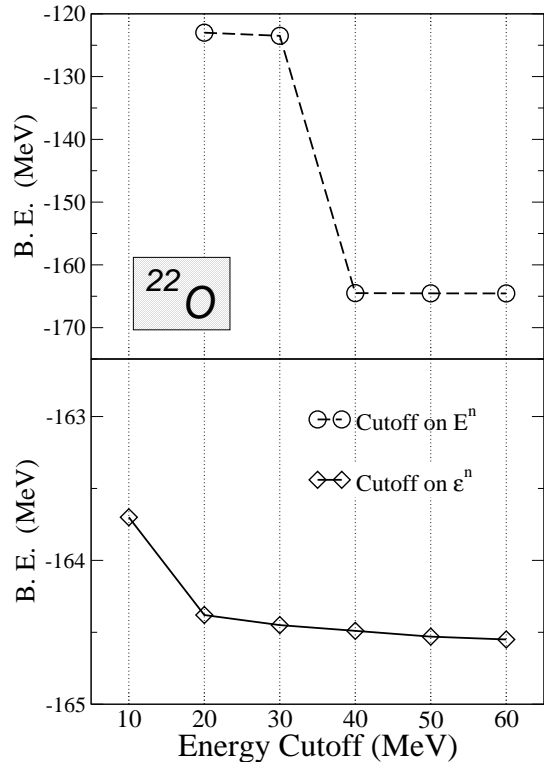


FIG. 1: Binding energy of ^{22}O vs. energy cutoff. Top: cutoff in the quasiparticle spectrum, bottom: cutoff in the equivalent single particle spectrum (absolute value). All calculations were performed with B-Spline order $M = 7$, $N_r = 18$ lattice points, angular momentum projection $\Omega_{max} = \frac{5}{2}$ and box size $R = 10fm$.

typically obtain quasiparticle energies up to about 1 GeV. It is well-known that zero-range pairing forces require a limited configuration space in the $p-p$ channel because the interaction matrix elements decrease too slowly with excitation energy [4]. One therefore introduces an energy cut-off, either in the quasiparticle energy (E_{max}) or in the equivalent single particle energy (\mathcal{E}_{max}). Hence, in the case of zero-range pairing forces the infinite summations over quasiparticle energies in the expressions for the densities ρ , τ , and current J are terminated at a maximum quasiparticle energy.

The quantity E_{max} has to be chosen such that the maximum quasiparticle energy exceeds the depth of the mean field nuclear potential, and all of the bound states have to be included in the sums [3]. We follow the prescription of Refs. [3, 23] to set the cutoff energy in terms of the equivalent single particle energy spectrum, \mathcal{E}_n . For the Skyrme SLy4 force with pure delta-pairing, Dobaczewski et al. [31] deduced a pairing strength of $V_0 = -170 \text{ MeV fm}^3$, with $\mathcal{E}_{max} = 60 \text{ MeV}$. We utilize the same parameters in all of our 2-D calculations.

Even though \mathcal{E}_{max} is a fixed parameter in the HFB calculations, it is interesting to analyze the sensitivity of observables to the value of the energy cutoff. In Fig. 1

we plot the total nuclear binding energy for cutoff values of \mathcal{E}_{max} between 10 and 60 MeV and the same for E_{max} from 20 to 60 MeV. We find that in both cases, the binding energy remains essentially constant for cutoff values of 40 MeV and above. Clearly, a cut-off below 40 MeV results in significant changes in the binding energy because quasiparticle levels with large occupation probabilities are left out. This result is in agreement with the 1-D radial calculations of Ref.[4].

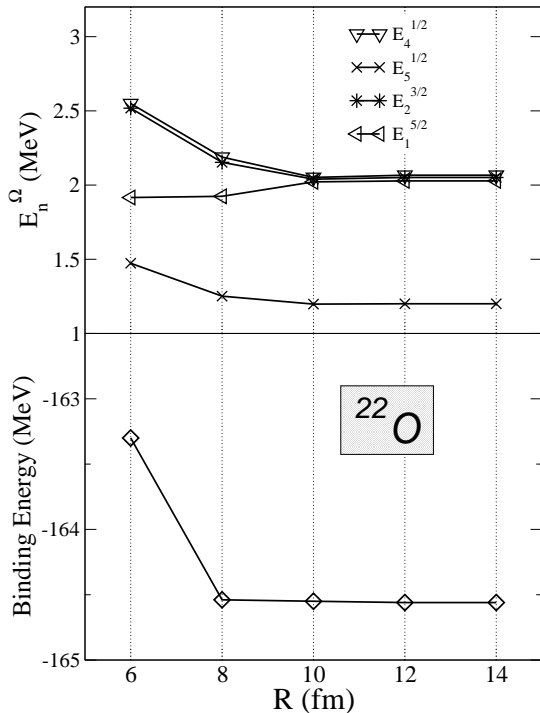


FIG. 2: Bottom: Total binding energy of ^{22}O as a function of the box size R . Top: Quasiparticle energies for states with large occupation probability (N_n) as a function of R . The spline order used was $M = 9$, $N_r = 19$ grid points, $\Omega_{max} = \frac{9}{2}$, and cutoff energy $\mathcal{E}_{max} = 60$ MeV.

B. Lattice box size

Using cylindrical coordinates, the lattice box size R defines the boundary in radial (r) direction; the box size in z direction is $2R$. The value of R must be chosen large enough for the wavefunctions to vanish at the outer edges of the box and needs to be adjusted for optimal accuracy and computing time. Figure 2 shows the dependence of the binding energy on R for ^{22}O . The mesh spacing was kept at a constant value of $\Delta r \approx 1fm$. Figure 2 also presents some of the quasiparticle energy levels E_n^Ω with large occupation probability N_n ; these levels correspond to low-lying states in the equivalent single-particle spectrum. Evidently, the quasiparticle energies and the total binding energy converge in essentially the same way with

increasing box size. Figure 2 shows that convergence is reached at $R=10$ fm. The behavior of the quasiparticle states with respect to the mesh boundaries has also been discussed in Ref. [4]. For heavier systems, the box size has to be increased. A safe initial guess for R is about three times the classical nuclear radius. Tests also show that one may utilize the same mesh spacing for both light and heavy nuclei.

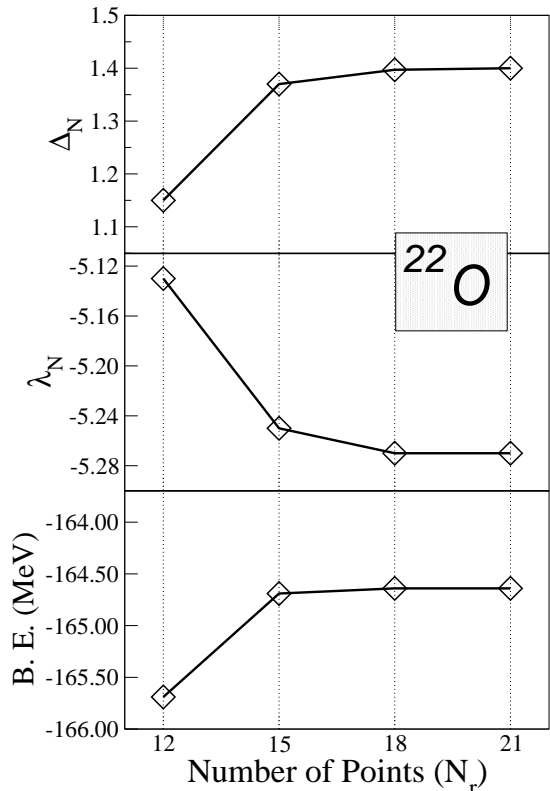


FIG. 3: Total binding energy, Fermi level and pairing gap for neutrons in ^{22}O vs. number of mesh points in radial direction, for fixed box size $R = 8$ fm. The quantities Ω_{max} and \mathcal{E}_{max} are the same as in Fig. 2

C. Number of mesh points

One of the major advantages of the B-Spline technique is that one can utilize a relatively coarse grid resulting in a lattice Hamiltonian matrix of low dimension. Fig. 3 shows several observables as a function of the number of radial mesh points, for a fixed box size $R = 8$ fm. The binding energy, neutron Fermi level, and pairing gap for ^{22}O reach their asymptotic values at about 18 grid points in radial direction. For the fixed (r, z) boundary conditions utilized in our work, the B-Spline lattice points show a (slightly) non-linear distribution, with more points in the vicinity of the boundaries. In the central region, the grid spacing for 18 radial points

is 0.75 fm.

D. Projection of the angular momentum, Ω

It has been mentioned in the formalism section that all observables can be expressed by sums over *positive* j_z quantum numbers $\Omega > 0$. The maximum value Ω_{max} increases, in general, with the number of protons and neutrons (Z, N) and also depends on the nuclear deformation. There is no *a priori* criterion to fix Ω_{max} ; this numerical parameter needs to be determined from test calculations in various mass regions. We have performed calculations for ^{22}O using Ω_{max} values from $5/2$ to $13/2$. Figure 4 displays the results for the total binding energy, neutron Fermi energy and neutron pairing gap. All three observables converge at $\Omega = 9/2$.

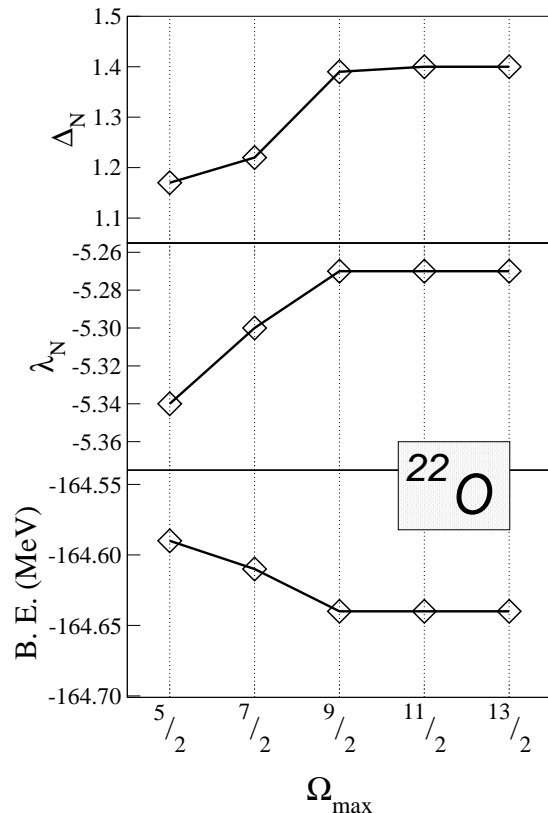


FIG. 4: Binding energy, neutron Fermi level, and average neutron pairing gap for ^{22}O vs. maximum angular momentum projection Ω_{max} . Box size $R = 10$ fm, $N_r = 18$ and an energy cutoff of 60 MeV were used.

VI. RESULTS

In this section we present converged numerical results of our 2D-HFB code. Our main goal is to demonstrate the accuracy of our Basis-Spline expansion technique on

a 2-D coordinate lattice by comparison with the 1-D coordinate space results of Dobaczewski et al. [4, 31] for spherical nuclei. For this purpose we have chosen two very neutron-rich spherical nuclei: a light nucleus, ^{22}O , with $N/Z = 1.75$ and a heavy system, ^{150}Sn , with $N/Z = 2.0$. Finally, we will also present results for a strongly deformed medium-heavy system, ^{102}Zr with $N/Z = 1.55$. This system was chosen because it allows us to compare our lattice results (which treat the continuum states accurately) to the “transformed harmonic oscillator” (THO) expansion technique recently developed by Stoitsov et al. [23]. In this framework, a local-scaling point transformation of the spherical harmonic oscillator is used to expand the quasiparticle wavefunctions in a set of bound single-particle wavefunctions.

A. Exotic spherical nuclei: ^{22}O and ^{150}Sn

In Table I we compare our 2-D HFB results for the spherical isotope ^{22}O with the 1-D radial HFB method of Ref.[3]. Corresponding results in the 2-D THO basis with 20 oscillator shells are also given. All calculations were performed with the Skyrme SLy4 force in the p-h channel and a pure delta interaction (strength $V_0 = -170\text{MeVfm}^3$) in the p-p channel, corresponding to volume pairing. The table lists several observables: the total binding energy (for comparison, the experimental value is -162.03MeV), the Fermi level for protons and neutrons, the neutron energy gap (for protons, the gap is exactly zero in all three calculations), the *rms* radius, and the quadrupole deformation (note that both 2-D calculations predict essentially zero deformation). Overall, the results of the axially symmetric code of the present work agree with the other two calculations in all the observables. The binding energy predicted by our 2D-lattice code is very close (within 40 keV) to the 1-D lattice result, while the THO method result differs by 80 keV. The difference in the Fermi level for protons is due to different conventions in choosing this energy for magic numbers. We choose the Fermi energy to be the

TABLE I: Calculations for ^{22}O for HFB+SLy4. The axially symmetric calculations (2D) of this work used a box size $R = 10\text{fm}$ with maximum $\Omega = \frac{9}{2}$ and an energy cutoff of 60 MeV. The spherical calculation of Ref. [31] was made with $R = 25\text{fm}$ and a $j = \frac{21}{2}$. All calculations were made with a cutoff at 60 MeV.

	1-D [31]	2-D (THO)[32]	2-D (this work)
B. E. (MeV)	-164.60	-164.52	-164.64
λ_n (MeV)	-5.26	-5.27	-5.27
λ_p (MeV)	-18.88	-18.85	-18.16
Δ_n (MeV)	1.42	1.41	1.40
Δ_p (MeV)	0.00	0.00	0.00
R_{rms} (fm)	2.92	2.92	2.92
β_2	*	0.00002	0.0008
$E_{pair}(n)$ (MeV)	-2.85	-2.78	-2.75

TABLE II: Comparison of calculations for spherical nucleus ^{150}Sn with HFB+SLy4. The 1-D calculations were made by Ref. [31], using a box size $R = 30$ and a linear spacing of points of 0.25 fm, with j_{max} of $\frac{21}{2}$. Calculations by the axially symmetric HFB 2-D code were made using a box size $R = 20\text{fm}$ with $N_r = 23$, maximum $\Omega = \frac{13}{2}$. In both calculations the pairing strength V_0 was set to -170 MeVfm^3 , and the energy cutoff to 60 MeV .

	1-D	2-D
B. E. (MeV)	-1129.0	-1129.6
λ_n (MeV)	-0.96	-0.94
λ_p (MeV)	-17.54	-17.69
Δ_n (MeV)	1.02	1.00
Δ_p (MeV)	0.00	0.02
R_{rms} (fm)	5.12	5.13
β_2	*	0.01
$E_{pair}(n)$ (MeV)	-10.452	-10.057

mid point of the energy of the last occupied level and the first unoccupied level.

We now present results for the tin isotope ^{150}Sn , a heavy nucleus far away from the valley of β -stability which is close to the two-neutron drip-line. Table II gives a comparison of our 2-D results (which predict a very small quadrupole deformation $\beta_2 = 0.005$) with Dobaczewski's 1-D radial HFB calculations. The box size used in the axially symmetric calculations was 20 fm in r direction and 40 fm in the z axis, whereas the 1-D code had a 30 fm radial box. Also, the density of points has a different meaning in the radial code, since it uses a different grid than the one used in the B-Splines technique for our 2-D code. For these calculations the resulting mesh spacing in the 1-D code was 0.25 fm, whereas the maximum mesh spacing in the 2-D one was 1.1 fm. In the 2-D calculations an approximately 3000×3000 matrix was diagonalized for each Ω and isospin value, and for each major HFB iteration. The full calculation required about 30 HFB iterations. Like in the oxygen isotope, the agreement is very good; a possible source of small discrepancies is the fact that our 2-D code yields $\beta_2 = 0.005$ whereas the 1-D code *assumes* an exactly spherical shape. Table II also contains another interesting piece of information on ^{150}Sn : the neutron Fermi level λ_n is located less than 1 MeV below the continuum which shows the proximity of this nucleus to the two-neutron dripline.

B. Deformed neutron-rich nucleus: ^{102}Zr

Our main motivation for developing an axially symmetric code is to perform highly accurate calculations for deformed nuclei, including the continuum states. The zirconium isotope ^{102}Zr is a heavy nucleus with strong prolate quadrupole deformation in its ground state. Its neutron to proton ratio of $N/Z = 1.55$ places it into the neutron-rich domain although it is likely far away from the neutron dripline (in the 1-D spherical HFB+SkP ap-

proximation [24] the last bound nucleus in the chain is predicted to be ^{136}Zr). We have chosen this isotope primarily because our results can be compared to the stretched harmonic oscillator expansion (THO) method mentioned above which does not involve any continuum states.

In Table III we present the results of our 2-D HFB calculations in coordinate space with the results obtained by the THO method. A comparison of the total binding energy of the system in both methods shows a difference of about 21 keV which can be considered small in comparison to the absolute value of the energy (the experimental binding energy value is -863.7 MeV). The pairing strength parameter, V_0 , used in each calculation also makes a difference. Other observables (Fermi levels, rms-radius and deformation β_2) agree quite well, also. However, we find differences in the energy gap values (Δ_n, Δ_p); these may be attributed to the different density of states used in the two methods see Eq. (2.25) or to the extrapolation of the oscillator parameter in the THO approach to deformed systems.

VII. CONCLUSIONS

In this paper, we have solved for the first time the *HFB continuum problem in coordinate space for deformed nuclei in two spatial dimensions* without any approximations. The novel feature of our new HFB code is that it takes into account high-energy continuum states with an equivalent single-particle energy of 60 MeV or more. In the past, this has only been possible in 1-D calculations for spherical nuclei [4]. Current 3-D HFB codes in coordinate space, e.g. Ref. [27], utilize an expansion of the quasiparticle wavefunctions in a truncated HF-basis which is limited to continuum states up to about 5 MeV of excitation energy.

The Vanderbilt HFB code has been specifically designed to study ground state properties of deformed axially symmetric even-even nuclei near the neutron and

TABLE III: Comparison of calculations *HFB + SLy4* for ^{102}Zr with two different methods in the axial symmetry. The configurational space calculations (THO) were made by Ref. [32] with 20 oscillator shells and pairing strength of -187.10 MeVfm^3 . Calculations by the coordinate space HFB 2-D code were made using a box size $R = 12\text{fm}$ with $N_r = 19$, maximum $\Omega = \frac{11}{2}$, V_0 -170 MeVfm^3 and the energy cutoff of 60 MeV .

	2-D (THO)	2-D (this work)
B. E. (MeV)	-859.40	-859.61
λ_n (MeV)	-5.42	-5.46
λ_p (MeV)	-12.10	-12.08
Δ_n (MeV)	0.56	0.31
Δ_p (MeV)	0.62	0.34
R_{rms} (fm)	4.58	4.58
β_2	0.429	0.431

proton drip lines. The large pairing correlations near the driplines and the strong coupling to the continuum represent major challenges for the numerical solution. We have solved the HFB problem on a two-dimensional grid in cylindrical coordinates (r, z) using a Basis-Spline representation of wavefunctions and operators. B-Splines are a generalization of the well-known finite element technique. By using B-Splines of order $M = 9$ (corresponding to polynomials of up to 8-th order) we are able to represent derivative operators very accurately on a relatively coarse grid with a lattice spacing of about 0.8 fm. While our current 2-D lattices are linear, a major advantage of the B-Spline technique is that it can be extended to non-linear lattices [15, 16] which will be particularly useful for an accurate and efficient calculation of neutron skins in heavy nuclei.

In this work, we have used the Skyrme (SLy4) effective N-N interaction in the p-h channel, and a pure delta interaction (corresponding to volume pairing) in the p-p channel. We present results for binding energies, deformations, normal densities and pairing densities, Fermi levels, and pairing gaps.

We have investigated the numerical convergence of several observables as a function of lattice box size, grid spacing, angular momentum Ω_{max} , and we have studied the sensitivity of the observables to the continuum cut-off. These test calculations were carried out for the neutron-rich isotope ^{22}O with $N/Z = 1.75$ which is close to the dripline nucleus ^{24}O .

Our HFB-2D code predicts a spherical shape for the neutron-rich nuclei ^{22}O and ^{150}Sn . In this case, our calculations can be compared with the 1-D radial HFB results of Dobaczewski et al. [4], and indeed there is good agreement between the two. We also present results for a strongly deformed system, ^{102}Zr , in which case we present a comparison with the stretched oscillator expansion method of Stoitsov et al. [23, 32].

We have implemented our code on an IBM-SP massively parallel supercomputer. Parallelization is possible for different angular momentum states Ω and isospins (p/n). We will also study alternative numerical techniques, in particular damping methods which we have utilized for solving the Dirac equation on a 3-D lattice [14].

In the near future, we plan to investigate several isotope chains, with particular concentration on deformed nuclei. We also plan to study a variety of Skyrme parameterizations for the mean field, and both volume and surface pairing. As more data from existing RIB facilities become available, it is likely that it will become necessary to develop new effective N-N interactions to describe these exotic nuclei. Furthermore, our 2-D HFB ground-state wavefunctions can be used as input into coordinate-space based QRPA calculations [33] to investigate collective excited states of nuclei near the driplines.

Acknowledgments

This work is supported by the U.S. Department of Energy under grant No. DE-FG02-96ER40963 with Vanderbilt University. Some of the numerical calculations were carried out on CRAY and IBM-SP supercomputers at the National Energy Research Scientific Computing Center (NERSC). We also like to acknowledge many fruitful discussions with W. Nazarewicz and M. Stoitsov (ORNL) and with J. Dobaczewski (Warsaw).

APPENDIX: SKYRME PARAMETERIZATION

The (density dependent) two-body effective N-N interaction is given by

$$\begin{aligned} v_{12}^{(2)} = & t_0 (1 + x_0 \hat{P}_\sigma) \delta(\mathbf{r}_1 - \mathbf{r}_2) \\ & + \frac{1}{2} t_1 (1 + x_1 \hat{P}_\sigma) \{ \delta(\mathbf{r}_1 - \mathbf{r}_2) \hat{k}^2 + \hat{k}'^2 \delta(\mathbf{r}_1 - \mathbf{r}_2) \} \\ & + t_2 (1 + x_2 \hat{P}) \hat{\mathbf{k}}' \cdot \delta(\mathbf{r}_1 - \mathbf{r}_2) \hat{\mathbf{k}} \\ & + \frac{1}{6} t_3 (1 + x_3 \hat{P}_\sigma) \rho^\gamma \delta(\mathbf{r}_1 - \mathbf{r}_2) \\ & + i W_0 (\hat{\sigma}_1 + \hat{\sigma}_2) \cdot \{ \hat{\mathbf{k}}' \times \delta(\mathbf{r}_1 - \mathbf{r}_2) \hat{\mathbf{k}} \}, \end{aligned}$$

\hat{P} being the exchange operator, and $\hat{\mathbf{k}}, \hat{\mathbf{k}}'$ relative momentum operators. This form of the interaction with parameters $x_0, x_1, x_2, x_3, t_0, t_1, t_2, t_3, t_4$, has been changed to an equivalent one with $b_1, b'_1, b_2, b'_2, b_3, b'_3, b_4, b'_4$, parameters [20]. This is done through the transformation

$$\begin{pmatrix} t_1 \\ t_1 x_1 \\ t_2 \\ t_2 x_2 \end{pmatrix} = \begin{pmatrix} 4/3 & 8/3 & -2/3 & -4/3 \\ -2/3 & -4/3 & 4/3 & 8/3 \\ 4 & -8/3 & 2 & -4/3 \\ -2 & 4/3 & -4 & 8/3 \end{pmatrix} \begin{pmatrix} b_1 \\ b_2 \\ b'_1 \\ b'_2 \end{pmatrix}. \quad (\text{A.1})$$

and

$$\begin{aligned} t_0 &= \frac{4}{3} b_0 - \frac{2}{3} b'_0 \\ t_0 x_0 &= -\frac{2}{3} b_0 + \frac{4}{3} b'_0 \\ t_3 &= \frac{16}{3} b_3 - \frac{8}{3} b'_3 \\ t_3 x_3 &= -\frac{8}{3} b_3 + \frac{16}{3} b'_3 \\ t_4 &= 2b_4 = 2b'_4. \end{aligned} \quad (\text{A.2})$$

The last equation only holds for certain forces, as shown in Table IV. For forces like SKI and SKO b_4 and b'_4 get different values.

1. Energy density

Calculation of the energy expectation value for an arbitrary interaction involves carrying out an integration

TABLE IV: Skyrme force parameters. Values for new parameters $b_0, b'_0, b_1, b'_1, b_2, b'_2, b_3, b'_3, b_4,$ and b'_4 have been calculated using relations A.1 and A.2, from old parameterization [18],[19], [20]. Numbers have been rounded to three decimal places.

Force	b_0	b'_0	b_1	b'_1	b_2	b'_2	b_3	b'_3	b_4	b'_4
SkM*	-2764.025	-1560.55	68.75	68.125	170.625	68.437	3898.75	1949.375	65.0	65.0
Z_σ	-3145.945	-3316.251	64.495	58.315	148.877	61.405	5577.823	6707.621	61.845	61.845
SkT6	-2145.863	-1600.426	0.0	0.0	110.25	0.0	4005.312	3204.25	53.5	53.5
SLy4	-3526.790	-3320.210	32.484	-49.289	185.325	62.665	5776.007	6385.639	61.5	61.5
SkI1	1000.310	869.809	32.354	-49.803	-432.059	-1136.719	580.693	-2810.714	62.13	62.13
SkI3	-2034.628	-1424.936	32.301	-127.914	100.074	-124.799	3336.309	3632.793	94.254	0.0
SkI4	-2231.708	-1679.676	32.271	-75.310	-121.462	-528.369	3814.977	3991.101	183.097	-180.351
SkP	-3359.948	-2322.346	44.642	89.284	190.343	140.223	5100.600	3185.341	50.0	50.0
SkO	-1882.032	-608.585	22.537	15.075	-72.754	-358.023	2660.027	237.585	176.578	-198.749
SkO'	-2068.449	-987.770	19.156	8.312	41.250	-128.648	3132.384	1192.344	143.895	-82.889

over six dimensions in coordinate space. One of the primary advantages of an interaction that contains a delta function, like the Skyrme one, is that the evaluation of such integral becomes substantially simplified, and it's reduced to a three-dimensional evaluation

$$E = \langle \Phi | H | \Phi \rangle = \int d^3r \mathcal{H}(\mathbf{r}) . \quad (\text{A.3})$$

The Hamiltonian density $\mathcal{H}(\mathbf{r})$ is composed of several terms

$$\mathcal{H} = \mathcal{H}_0 + \mathcal{H}_{LS} + \mathcal{H}_C . \quad (\text{A.4})$$

The kinetic energy and some of the density dependent terms in the Skyrme interaction are included in

$$\begin{aligned} \mathcal{H}_0 = & \frac{\hbar^2}{2m} \tau + \frac{b_0}{2} \rho^2 - \frac{b'_0}{2} \sum_q \rho_q^2 \\ & + \frac{b_3}{3} \rho^{\alpha+2} - \frac{b'_3}{3} \rho^\alpha \sum_q \rho_q^2 \\ & + b_1 (\rho\tau - j^2) - b'_1 \sum_q (\rho_q \tau_q - j_q^2) \\ & - \frac{b_2}{2} \rho \nabla^2 \rho + \frac{b'_2}{2} \sum_q \rho_q \nabla^2 \rho_q . \end{aligned} \quad (\text{A.5})$$

The current densities (\mathbf{j}, \mathbf{j}_q) appearing in this term are identically zero for time independent states. The finite range spin-orbit terms have the form

$$\mathcal{H}_{LS} = -b_4 \rho \nabla \cdot \mathbf{J} - b'_4 \sum_q \rho_q (\nabla \cdot \mathbf{J}_q) . \quad (\text{A.6})$$

The Coulomb term contains an integral over the proton density as well as the Slater exchange term,

$$\begin{aligned} \mathcal{H}_C = & \frac{e^2}{2} \int d^3r' \rho_p(\mathbf{r}) \frac{1}{|\mathbf{r} - \mathbf{r}'|} \rho_p(\mathbf{r}') \\ & - \frac{3}{4} e^2 \left(\frac{3}{\pi} \right)^{1/3} [\rho_p(\mathbf{r})]^{4/3} . \end{aligned} \quad (\text{A.7})$$

2. Single Particle Hamiltonian

The Hartree-Fock Hamiltonian using the Skyrme effective interaction can be written as

$$\begin{aligned} h_q = & - \nabla \cdot \frac{\hbar^2}{2m_q^*} \nabla + U_q + U_C \cdot \delta_{q,p} \\ & + \frac{1}{2i} (\nabla \cdot \mathbf{I}_q + \mathbf{I}_q \cdot \nabla) - i \mathbf{B}_q \cdot (\nabla \times \sigma) . \end{aligned} \quad (\text{A.8})$$

Several effective quantities appear in this equation. The effective mass is defined by

$$\frac{\hbar^2}{2m_q^*} = \frac{\hbar^2}{2m} + b_1 \rho - b'_1 \rho_q , \quad (\text{A.9})$$

the effective current density

$$\mathbf{I}_q = -2 b_1 \mathbf{j} + 2 b'_1 \mathbf{j}_q , \quad (\text{A.10})$$

and the effective spin density

$$\mathbf{B}_q = b'_1 \mathbf{J}_q + b_4 \nabla \rho + b'_4 \nabla \rho_q . \quad (\text{A.11})$$

As previously indicated, all of the terms in Eq.(A.10) vanish for bound states. Also, the first term in Eq.(A.11) is usually ignored.

The effective nuclear potential for the Skyrme force is given by

$$\begin{aligned} U_q = & b_0 \rho - b'_0 \rho_q + b_1 \tau - b'_1 \tau_q \\ & + \frac{b_3}{3} (\alpha + 2) \rho^{\alpha+1} - \frac{b'_3}{3} \left[\alpha \rho^{\alpha-1} \sum_q \rho_q^2 + 2 \rho^\alpha \rho_q \right] \\ & - b_4 \nabla \cdot \mathbf{J} - b'_4 \nabla \cdot \mathbf{J}_q \\ & + b'_2 \nabla^2 \rho_q - b_2 \nabla^2 \rho , \end{aligned} \quad (\text{A.12})$$

and the Coulomb field is

$$U_C = e^2 \int d^3r' \frac{\rho_p(\mathbf{r}')}{|\mathbf{r} - \mathbf{r}'|} - e^2 \left(\frac{3}{\pi} \right)^{1/3} [\rho_p(\mathbf{r})]^{1/3} . \quad (\text{A.13})$$

\mathcal{B}_r and \mathcal{B}_z from equations (3.13) for the spin-orbit part representation of the potential operator are given by:

$$\mathcal{B}_r \equiv \mathbf{B}_q \cdot \mathbf{e}_r = \nabla_r (b_4 \rho + b'_4 \rho_q) \quad (\text{A.14a})$$

$$\mathcal{B}_z \equiv \mathbf{B}_q \cdot \mathbf{e}_z = \nabla_z (b_4 \rho + b'_4 \rho_q) , \quad (\text{A.14b})$$

b_4 and b'_4 values are shown in Table IV for different forces.

-
- [1] "Scientific Opportunities with an Advanced ISOL Facility", Panel Report (Nov. 1997), ORNL.
- [2] "RIA Physics White Paper", RIA 2000 Workshop, Raleigh-Durham, NC (July 2000), distributed by NSCL, Michigan State University.
- [3] J. Dobaczewski, H. Flocard and J. Treiner, Nucl. Phys. **A422**, 103 (1984).
- [4] J. Dobaczewski, W. Nazarewicz, T.R. Werner, J.F. Berger, C.R. Chinn and J. Dechargé, Phys. Rev. **C53**, 2809 (1996).
- [5] P. Navratil, B.R. Barrett and W.E. Ormand, Phys. Rev. **C 56**, 2542 (1997).
- [6] S.E. Koonin, D.J. Dean and K. Langanke, Phys. Rep. **1**, 278 (1997).
- [7] K.T.R. Davies, K.R.S. Devi, S.E. Koonin and M.R. Strayer, in *Treatise on Heavy Ion Science*, edited by D.A. Bromley (Plenum, New York, 1985), Vol. 3, p. 3.
- [8] J.W. Negele, Rev. Mod. Phys. **54**, 913 (1982).
- [9] B.D. Serot, Rep. Prog. Phys. **55**, 1855 (1992).
- [10] P. Ring, Prog. Part. Nucl. Phys. **37**, 193 (1996).
- [11] W. Pöschl, D. Vretenar, G.A. Lalazissis and P. Ring, Phys. Rev. Lett. **79**, 3841 (1997).
- [12] P. Ring and P. Schuck, "The Nuclear Many-Body Problem", (Springer Verlag, New York, 1980).
- [13] A.S. Umar, J. Wu, M.R. Strayer and C. Bottcher, J. Comp. Phys. **93**, 426 (1991).
- [14] J.C. Wells, V.E. Oberacker, M.R. Strayer and A.S. Umar, Int. J. Mod. Phys. **C6**, 143 (1995).
- [15] D.R. Kegley, Ph.D. thesis, Vanderbilt University (1996).
- [16] D.R. Kegley, V.E. Oberacker, M.R. Strayer, A.S. Umar and J.C. Wells, J. Comp. Phys. **128**, 197 (1996).
- [17] V.E. Oberacker and A.S. Umar, in "Perspectives in Nuclear Physics" (ed. J.H. Hamilton, H.K. Carter and R.B. Piercey), World Scientific Publ. Co. (1999), p. 255-266.
- [18] D. Vautherin and D.M. Brink, Phys. Rev. **C 5**, 626 (1972).
- [19] J. Bartel, P. Quentin, M. Brack, C. Guet and H.B. Håkansson, Nucl. Phys. **A386**, 79 (1982).
- [20] P.-G. Reinhard, D.J. Dean, W. Nazarewicz, J. Dobaczewski, J. A. Maruhn and M.R. Strayer, Phys. Rev. **C 60**, 014316 (1999).
- [21] J. Dobaczewski, W. Nazarewicz and T.R. Werner, Phys. Scr. **T56**, 15 (1995).
- [22] E. Chabanat, P. Bonche, P. Haensel, J. Meyer and R. Schaeffer, Nucl. Phys. **A635**, 231 (1998); Nucl. Phys. **A643**, 441 (1998).
- [23] M.V. Stoitsov, J. Dobaczewski, P. Ring and S. Pittel, Phys. Rev. **C 61**, 034311 (2000).
- [24] R. Smolańczuk and J. Dobaczewski, Phys. Rev. **C48**, R2166 (1993).
- [25] J.L. Egido and L.M. Robledo, Phys. Rev. Lett. **70**, 2876 (1993).
- [26] A. Petrovici, K.W. Schmid, F. Grümmer and A. Faessler, Nucl. Phys. **A517**, 108 (1990).
- [27] J. Terasaki, P.-H. Heenen, H. Flocard and P. Bonche, Nucl. Phys. **A600**, 371 (1996).
- [28] W. Nazarewicz, J. Dobaczewski, T.R. Werner, J.A. Maruhn, P.-G. Reinhard, K. Rutz, C.R. Chinn, A.S. Umar and M.R. Strayer, Phys. Rev. **C 53**, 740 (1996).
- [29] C.R. Chinn, J.-F. Berger, D. Gogny and M.S. Weiss, Phys. Rev. **C45**, 1700 (1992).
- [30] P.-H. Heenen and R.V.F. Janssens, Phys. Rev. **C57**, 159 (1998).
- [31] J. Dobaczewski (private communication).
- [32] M. V. Stoitsov (private communication).
- [33] M. Matsuo, Nucl. Phys. **A696**, 371 (2001).